**FORSCHUNGSZENTRUM JÜLICH GmbH**
**Zentralinstitut für Angewandte Mathematik**
**D-52425 Jülich, Tel. (02461) 61-6402**

Interner Bericht

# Shakedown and ratchetting under tension-torsion loadings: analysis and experiments

*M. Heitzer, M. Staat, H. Reiners, F. Schubert*

FZJ-ZAM-IB-2003-03

März 2003

(letzte Änderung: 19.03.2003)

Preprint: submitted for publication

# Shakedown and ratchetting under tension-torsion loadings: analysis and experiments

M. Heitzer[1], M. Staat[2], H. Reiners[3], F. Schubert[3]

[1]*Central Institute for Applied Mathematics (ZAM), Forschungszentrum Jülich, D–52425 Jülich, Germany*

[2]*FH–Aachen Div. Jülich, Ginsterweg 1, D-52428 Jülich, Germany*

[3]*Institute for Materials and Processes in Energy Systems (IWV) Forschungszentrum Jülich GmbH D-52425 Jülich, Germany*

SUMMARY

Structural design analyses are conducted with the aim of verifying the exclusion of ratchetting. To this end it is important to make a clear distinction between the shakedown range and the ratchetting range. The performed experiment comprised a hollow tension specimen which was subjected to alternating axial forces, superimposed with constant moments. First, a series of uniaxial tests has been carried out in order to calibrate a bounded kinematic hardening rule. The load parameters have been selected on the basis of previous shakedown analyses with the PERMAS code using a kinematic hardening material model. It is shown that this shakedown analysis gives reasonable agreement between the experimental and the numerical results. A linear and a nonlinear kinematic hardening model of two-surface plasticity are compared in material shakedown analysis.

## 1. Introduction

Structural design of passive structures in the apparatus engineering are based on the analysis of plastic limit states. The new European Standard for pressure vessel and boiler design contains the proposal of the European Pressure Equipment Research Council (EPERC) for Design-by-Analysis (DBA) to exclude ratchetting and therefore the limitation of progressive plastic deformation (Taylor et al., 1999). The more traditional DBA routes in the major codes and standards in the pressure equipment field (including the ASME Pressure Vessel and Boiler Code) try to estimate the plastic behaviour from an extrapolation of an elastic stress analysis. This way runs into the stress classification problem which lacks a rational solution (Taylor et al., 1999).

In the future FEM-based shakedown analyses will be needed for DBA, which can guaranty a uniform safety assessment for complex structures. For perfectly plastic materials and simple load cases shakedown analyses are performed for different pressure vessel problems (Taylor et al., 1999). In the European project LISA general limit and shakedown analyses for kinematic hardening material are developed and implemented in the general purpose FEM code PERMAS (Staat and Heitzer, 2001). For the validation of the shakedown theory for hardening material there is a shortage of tests involving cyclic, mechanical and thermal loads at the limit between shakedown and ratchetting, but a lot of experiments to test different hardening laws, e.g. (Portier et al. 2000), (Bari 2001). Two-bar and multi-bar tests (Ponter, 1983), (Lang et al., 2001), like the Bree problem, enable representation of simple mechanical models of pipes and vessels subjected to internal pressure and a temperature gradient across the wall thickness. The tests presented here are aimed at determining the elastic shakedown limit, below which failure due to ratchetting has not to be assumed.

Structural ratchetting or shakedown are different responses to the cyclic loading which depend on

the development of inhomogeneous residual stress fields. In torsion experiments the stress is the more homogeneous the thinner the tube wall is. For homogeneous stress fields the ratchetting is caused by the material behaviour alone (Hübel, 1996). Ratchetting experiments with uniaxial and biaxial stress cycles have been used to improve constitutive modeling for cyclic plasticity. In these experiments the Melan and Prager linear kinematic hardening law is found to be inadequate to simulate material ratchetting, because it always stabilizes to shakedown of homogeneous stress fields after some initial over-prediction of ratchetting (Bari, 2001). The tension torsion experiment is situated between material and structural ratchetting and may therefore give some hints on the reliability of shakedown analyses if ratchetting is not controlled by stress inhomogeneity.

In (Heitzer and Staat, 1999) a technique was applied which calculates the collapse and shakedown load of ductile structures directly on the basis of FEM discretization, without stress classification. This technique could be extended in (Heitzer et al., 2000) to bounded kinematic hardening material. This paper describes a test carried out using this technique, and draws a comparison with the results of the shakedown analysis and the experimental results. Some material ratchetting analyses are used to assess the effects of nonlinear kinematic hardening models on the shakedown behaviour of structures with little redundancy.

## 2. Test specimen and experimental results

### 2.1. Geometry and material

The material chosen for this study is the ferritic steel 20 MnMoNi 5 5, often used as material for the pressure boundary of nuclear power plants. The chemical composition of the material is given in Tab. 1. Tensile specimens for uniaxial load tests were machined from a 500 mm x 1000 mm block. The geometry of the specimens is given in Fig. 1. In order to characterize the mechanical behaviour of the material, mainly the stress strain behaviour under uniaxial loading, two uniaxial tests were performed on a INSTRON 1343 servohydraulic test machine. The same test equipment operating in biaxial strain or in biaxial stress was controlled with load cell of type LEBOW. An INSTRON extensometer was used to monitor axial strains (Fig. 2). A PC 486 computer equipped with CASYLAB 5.0 software controlled the acquisition operations and command signal generation. In addition the torsion angle was recorded.

**Table 1:** Chemical composition of 20 MnMoNi 5 5 (% in weight)

| C | Si | Mn | P | S | Cr | Mo | Ni | V |
|---|---|---|---|---|---|---|---|---|
| 0.24 | 0.24 | 1.38 | 0.002 | 0.002 | 0.09 | 0.51 | 0.80 | ¡0.01 |

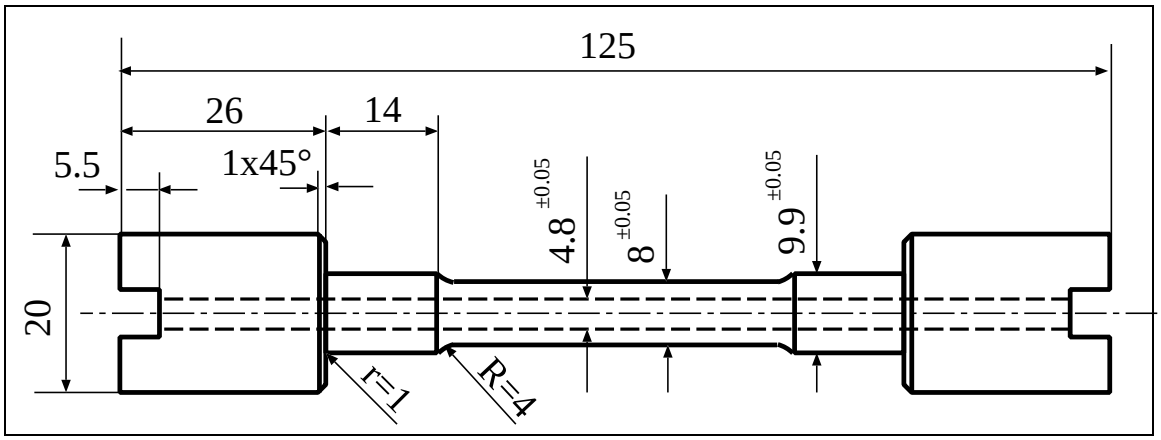


**Figure 1:** Geometry and sizes of the test specimens

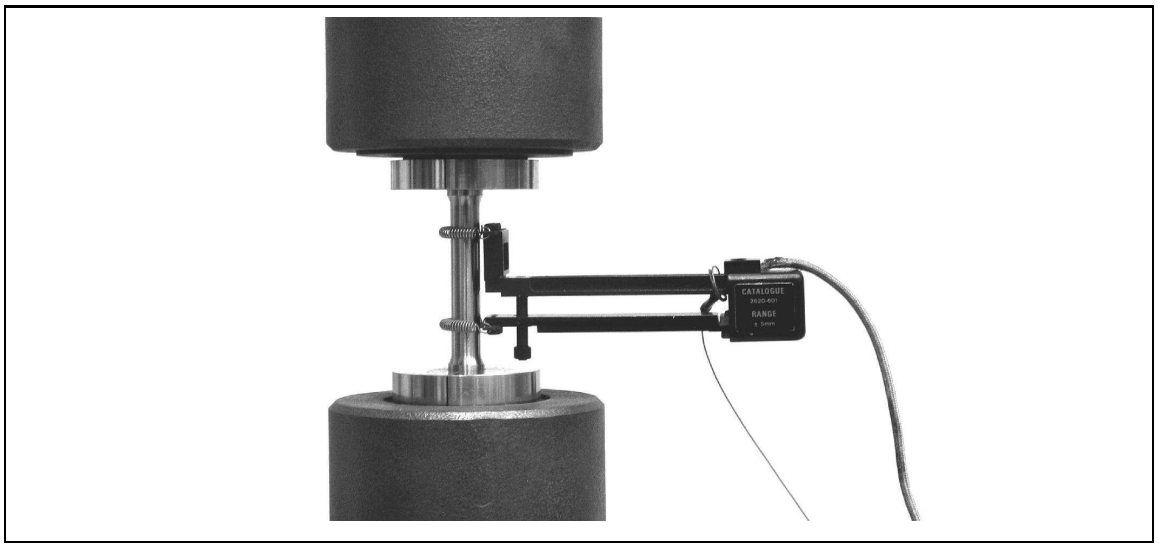


**Figure 2:** Experimental equipment

## 2.2. Description of the loadings and experimental results

First, the strain hardening of the material under monotonic loading was characterized. Fig. 3 shows the corresponding stress-strain curves. The tested material properties, lower yield stress $\sigma_y$, ultimate stress $\sigma_u$, Young's modulus $E$ and Poisson's ratio $\nu$ are summarized in Tab. 2.

**Table 2:** Definition of the material properties obtained by tensile testing

| $\sigma_y$ | $\sigma_u$ | E | $\nu$ |
|---|---|---|---|
| $485N/mm^2$ | $631N/mm^2$ | $2.07 \cdot 10^5 N/mm^2$ | 0.3 |

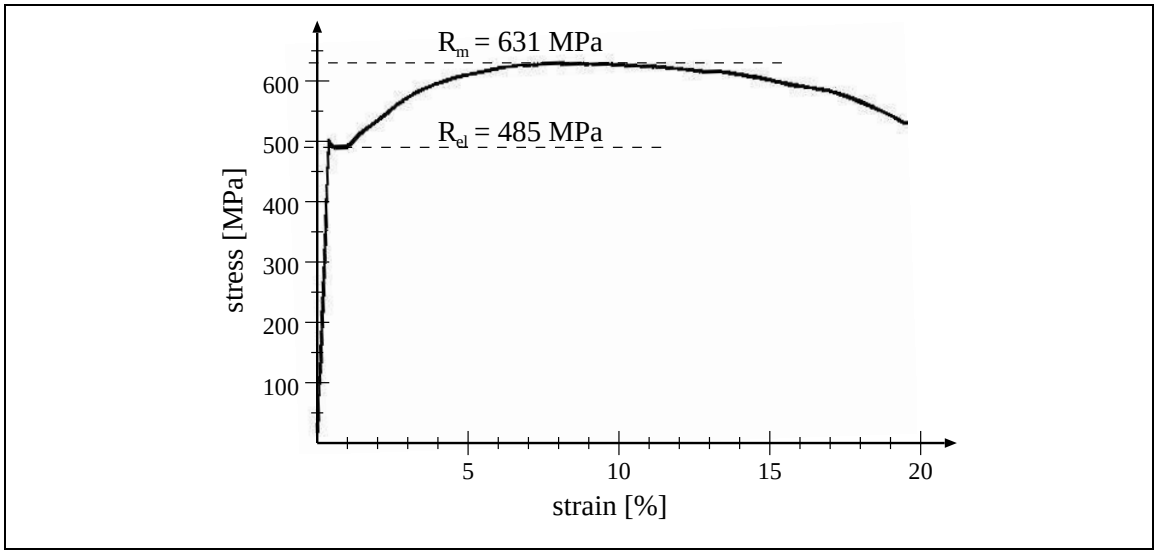


**Figure 3:** Stress-strain curve

## 2.3. Experimental investigations of biaxial tension-torsion loadings

The ratchetting behaviour was studied with a tension-torsion test under axial stress control. 10 experiments were performed to verify the shakedown domain for the tension-torsion loading regime calculated by the kinematic hardening approach presented in section 4.5. The load matrix of the experiments is given in Tab. 3. The mean values of the tension load are given in Tab. 3 and for all experiments an amplitude of $\pm\Delta\sigma = 1$ kN is chosen. The remaining enlargement and the torsion angle of the specimens are given in addition in Tab. 3. The cyclic 'creep' is shown in Fig. 4, i.e. the torsion angle increases for constant moment loading. In the case of unbounded increase incremental collapse is reached, whereas the torsion angle stabilizes for elastic shakedown Fig. 5.

**Table 3:** Loading, deformation and torsion angle of the experiments

| experiment | 1 | 2 | 3 | 4 | 5 | 6 | 7 | 8[1] | 9 | 10 |
|---|---|---|---|---|---|---|---|---|---|---|
| tension [kN] | 17 | 15 | 16 | 10 | 18 | 21 | 17 | 20 | 18 | 5 |
| moment [Nm] | 7 | 21 | 14 | 28 | 17 | 4 | 24 | 14 | 3 | 32 |
| number of cycles | 150 | 100 | 100 | 71 | 100 | 100 | 200 | 200 | 200 | 200 |
| angle [°] | 10.6 | 25.0 | 16.1 | 24.9 | 22.9 | 10.6 | 43.9 | 25.7 | 4.7 | 10.9 |
| axial strain | 0.11 | 0.097 | 0.313 | 0.931 | 0.786 | 2.362 | 1.075 | 1.328 | 0.092 | 0.077 |

[1] Initial overload up to 22 kN.

In the framework of the classical plasticity theory the results of the shakedown analysis are independent of the load history. Therefore, the specimens No. 1 and 3 are used again for the experiments 9 and 10, respectively. Specimen No.8 was loaded in the first step up to 22 kN. After a stabilization period the specimen was loaded by the given load history, such that the remaining deformation after the loading has to be reduced to investigate the real cyclic behaviour. The initial overload was lower than the limit load such that the ratchetting behaviour of the specimen is still predominant.

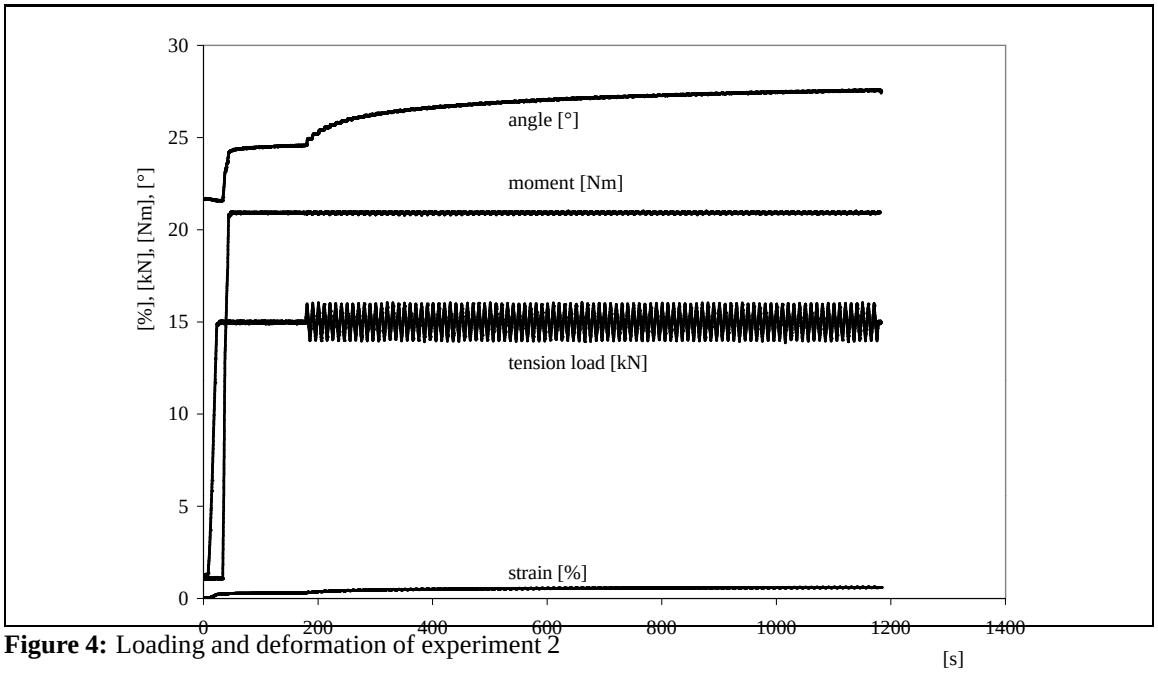


**Figure 4:** Loading and deformation of experiment 2

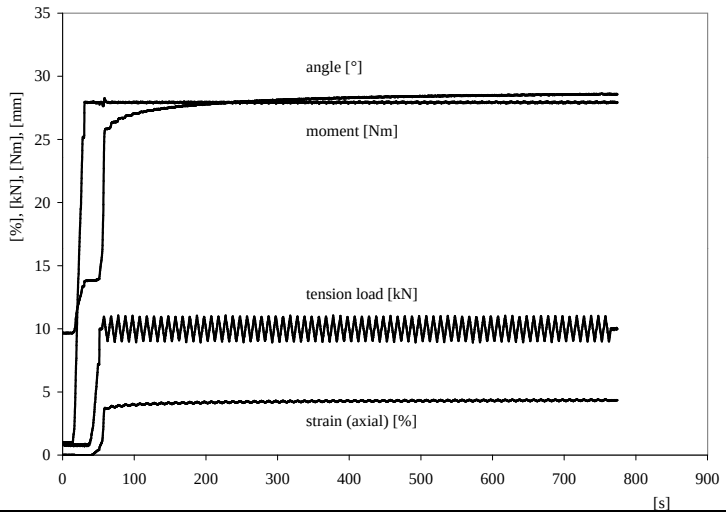


**Figure 5:** Loading and deformation of experiment 4

# 3. Theory and numerical results

## 3.1. Perfectly plastic shakedown formulation

Depending on the loading a structure shows different structural responses. For time-variant loading the structure can fail plastically in addition to the plastic collapse at limit load by:

- incremental collapse by accumulation of plastic strains in successive load cycles (ratchetting, progressive plastification, cyclic 'creep')
- plastic fatigue by alternate plastification in few load cycles (Low Cycle Fatigue (LCF), plastic shakedown).

The structure does not fail plastically, if finally all plastic strain rates vanish and the dissipated energy remains finite. One says that the structure adapts to the load or it shakes down elastically. After few initially plastic cycles no difference to the purely elastic behaviour can be observed in structural mechanics quantities. Shakedown analysis considers only the asymptotic structural response. Infinite accumulation of plastic deformation is called ratchetting. If accumulation ends with finite values after some transient ratchetting it is denoted shakedown (in the sense of finite ratchetting).

The time history of a load $\boldsymbol{P}(t) = (\boldsymbol{q}(t), \boldsymbol{p}(t))$ with body forces $\boldsymbol{q}$ and surface loads $\boldsymbol{p}$ is often not well-known. It can however usually be stated that the loads (e.g. mechanical and thermal loads) vary only within a certain convex load domain $\mathcal{L}$. Typically, $\mathcal{L}$ is given by amplitudes or admissible bounds. If $N_L$ is the number of vertices $\boldsymbol{P}_1, \ldots, \boldsymbol{P}_{N_L}$ of $\mathcal{L}$, then all loads $\boldsymbol{P}(t) \in \mathcal{L}$ can be represented as convex combination

$$\boldsymbol{P}(t) = \lambda_1(t)\boldsymbol{P}_1 + \ldots + \lambda_{N_L}(t)\boldsymbol{P}_{N_L}, \ \sum_{j=1}^{N_L} = \lambda_j(t) = 1, \ \ 0 \leq \lambda_j(t) \leq 1.$$

The load-carrying capacity is exhausted by enlargement of $\mathcal{L}$ with the factor $\alpha > 1$ causing LCF, ratchetting or collapse. The shakedown theory analyzes only the shakedown state, i.e. it answers the question, whether a structure from ductile material is plastically safe or not. With a static criterion, a structure under a load range $\mathcal{L}$ shakes down, if for each load in $\mathcal{L}$ an admissible stress field can be found which is in equilibrium with this load. A stress field is admissible if it fulfills the yield condition with the yield function $F$. For perfectly plastic material this corresponds to $F[\boldsymbol{\sigma}_j] \leq \sigma_y^2$ with the yield stress $\sigma_y$, where the square of the von Mises yield function $F[\boldsymbol{\sigma}] = 3/2\ \boldsymbol{\sigma}^D : \boldsymbol{\sigma}^D$ with the deviatoric stress $\boldsymbol{\sigma}^D$ is used. It is sufficient to satisfy the shakedown conditions only in

the $N_L$ vertices $\boldsymbol{P}_1, \ldots, \boldsymbol{P}_{N_L}$ of $\mathcal{L}$ if $\mathcal{L}$ is a convex set, because the shakedown theorems lead to convex optimization problems.

**Static shakedown theorem:**

A structure $V$ shakes down under a convex load domain $\alpha\mathcal{L}$, if for any basis load $\alpha\boldsymbol{P}_j$ an admissible stress field $\boldsymbol{\sigma}_j$ can be found, which is in equilibrium with $\alpha\boldsymbol{P}_j$. In formulae:

$$\begin{aligned} F[\boldsymbol{\sigma}_j] &\leq \sigma_y^2 && \text{in} \quad V, \;\; j = 1, \ldots, N_L \\ -\text{div}\boldsymbol{\sigma}_j &= \alpha \boldsymbol{q}_j && \text{in} \quad V, \;\; j = 1, \ldots, N_L \\ \boldsymbol{\sigma}_j \, \mathbf{n} &= \alpha \boldsymbol{p}_j && \text{on} \quad \partial V_\sigma, \;\; j = 1, \ldots, N_L. \end{aligned} \tag{1}$$

For kinematic hardening material the stresses still have to be in equilibrium with the applied forces, but the formulation of the yield condition is more complicated than for perfectly plastic material law. The static theorem leads to a save lower bound, whereas the upper bound is obtained by a kinematic approach (Staat and Heitzer, 2001).

## 3.2. Kinematic hardening formulation

The linear kinematic hardening corresponds to the translation of the loading surface in the multiaxial loading space:

$$F[\boldsymbol{\sigma} - \boldsymbol{\pi}] = \sigma_y^2. \tag{2}$$

The interior of the loading surface $\left\{\boldsymbol{\sigma} \mid F[\boldsymbol{\sigma} - \boldsymbol{\pi}] < \sigma_y^2\right\}$ is the elastic domain which is described by the function $F$ and the yield stress $\sigma_y$.

For realistic materials the stress $\boldsymbol{\sigma}$ is bounded by the ultimate stress $\sigma_u$. Therefore, the displacement of the initial yield surface is bounded. The hardening is bounded, if the displacement of the initial yield surface is bounded within a bounding surface in the stress space. Within a simple formulation the bounding surface is described by the same von Mises function:

$$F[\boldsymbol{\sigma}] \leq \sigma_u^2. \tag{3}$$

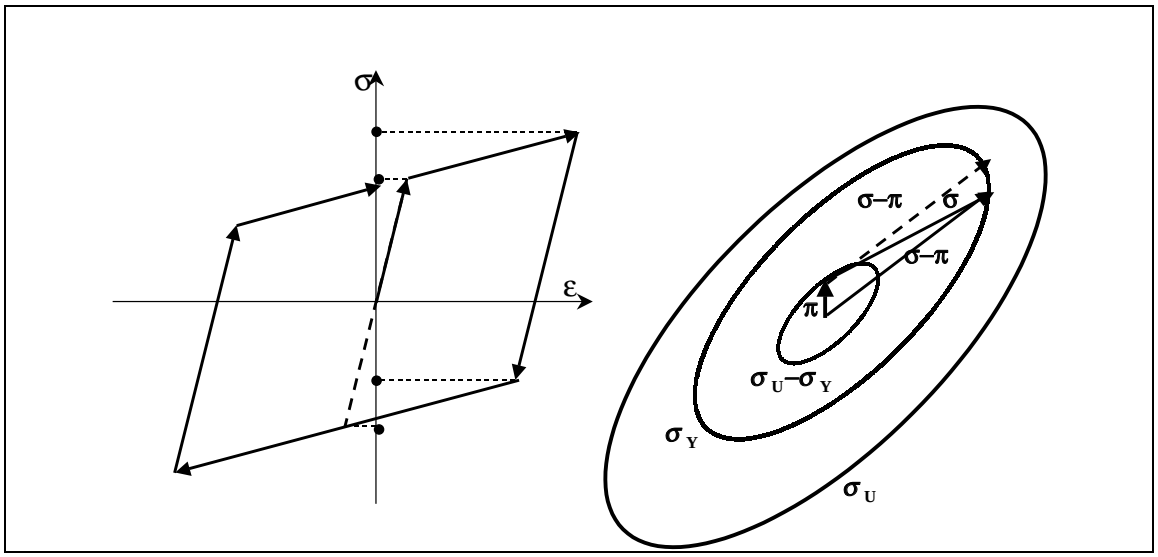


**Figure 6:** Two-surface model of bounded kinematic hardening, uni- and multiaxial below saturation

The limit stress $\sigma_u$ is set to $R_m$ if the hardening effect is regarded totally. The elastic domain remains always in the limit surface and any stress $\boldsymbol{\sigma}$ in it may be reached if and only if (Fig. 6)

$$F[\boldsymbol{\pi}] \leq (\sigma_u - \sigma_y)^2. \tag{4}$$

In the literature more advanced hardening models exist with much more details, but they may not be needed for the decision if a structure shakes down or not. In the Besseling overlay material model the shakedown behaviour is described only by $\sigma_u$ and $\sigma_y$ (Stein et al., 1993). Pycko and Maier (1995) and De Saxce et al. (2000) extended the shakedown theory to the advanced Armstrong and Frederick hardening law.

### 3.3. Shakedown formulation for kinematic hardening material

The extended static theorem of shakedown for a bounded kinematic hardening material can be formulated as follows (Stein et al., 1993), (Heitzer et al., 2000):

> If there exist a time–independent backstress field $\boldsymbol{\pi}$ satisfying
>
> $$F[\boldsymbol{\pi}] \leq (\sigma_u - \sigma_y)^2, \qquad \text{in} \quad V \tag{5}$$
>
> a factor $\alpha > 1$ and a time–independent residual stress field $\boldsymbol{\rho}$ such that
>
> $$F[\alpha \boldsymbol{\sigma}^E(t) + \boldsymbol{\rho} - \boldsymbol{\pi}] \leq \sigma_y^2 \qquad \text{in} \quad V \tag{6}$$
>
> holds for all possible loads $\mathbf{P}(t) \in \mathcal{L}$ and for all material points, then the structure will shake down elastically under the given convex load domain $\mathcal{L}$.

The greatest value $\alpha_{sd}$ for which the theorem holds is called shakedown-factor. This lower bound approach leads to the convex optimization problem

$$\begin{aligned}
\max \quad & \alpha && && (7)\\
\text{s.t.} \quad & F[\alpha \boldsymbol{\sigma}_j^E + \boldsymbol{\rho} - \boldsymbol{\pi}] \leq \sigma_y^2 && \text{in} \quad V, \;\; j = 1, \ldots, N_L && (8)\\
& F[\boldsymbol{\pi}] \leq (\sigma_u - \sigma_y)^2 && \text{in} \quad V && (9)\\
& \operatorname{div} \boldsymbol{\rho} = \mathbf{0} && \text{in} \quad V && (10)\\
& \boldsymbol{\rho}\, \mathbf{n} = \mathbf{0} && \text{on} \quad \partial V_\sigma && (11)
\end{aligned}$$

with infinitely many constraints, which can be reduced to a finite problem by FEM discretization. If the load regime $\mathcal{L}$ shrinks to a single load point, limit analysis is obtained as a special case. For the perfectly plastic behavior ($\sigma_u = \sigma_y$), the backstresses $\boldsymbol{\pi}$ are identical zero due to inequality (9). Melan's original theorem (Melan, 1938) for unbounded kinematic hardening can also be deduced from the previous formulation if $\sigma_u \to \infty$. Then inequality (9) is not relevant anymore and the backstresses $\boldsymbol{\pi}$ are free variables.

### 3.4. Discretization and Optimization

The shakedown theorems formulated for the continuum can be discretized by the FEM or they can be deduced directly for a discretized structure. For the FEM the structure $V$ is decomposed in $NE$ finite elements with the $NG$ Gaussian points. The constraints of the optimization problem are satisfied only in the Gaussian points.

The number of Gaussian points becomes huge for industrial structures and no effective solution algorithms for the nonlinear optimization problem are available. A method for handling such large–scale optimization problems called basis reduction technique, was used in (Stein et al., 1993), (Heitzer, 1999), (Heitzer et al., 2000). This basis reduction technique generalizes the line search technique, well–known in optimization theory (Fletcher, 1987). Instead of searching the whole feasible region for the optimum a search direction (a subspace with a small dimension) is chosen and one searches for the best value in this direction. The basis of the subspaces are generated by the general purpose Finite Element Code PERMAS (Heitzer and Staat, 1999), (Intes, 1988). The

basis reduction and the subspace iteration technique described (Heitzer, 1999), (Stein et al., 1993) for perfectly plastic material cannot be directly applied to the shakedown problem for bounded kinematic hardening model. Therefore, Heitzer et al. (2000) proposed a method applicable with arbitrary three–dimensional finite elements for bounded kinematic hardening material law.

# 4. Analytical and numerical structural shakedown analysis

The experiment comprised a hollow tension specimen which was subjected to alternating axial tension with nonzero mean stress and constant moments. An analytical solution is given for the hollow part of the specimen, i.e. a pipe with inner radius $R_i$ and outer radius $R_a$ is investigated. For simplicity of presentation the unbounded Melan and Prager linear kinematic hardening model is used. The comparison with the experiments is made against more realistic shakedown analyses with the FEM using a bounded Melan and Prager model.

## 4.1. Elastic analysis

For pure torsion and axial symmetry the normal stresses vanishes and only shear stresses $\tau(r) = \sigma_{\theta z}$ occur. The elastic stresses for constant moment $M_z$ at the radius $r$ are

$$\boldsymbol{\sigma}_M(r) = (0, 0, 0, \tau(r))^T \text{ with } \tau(r) = \frac{2M_z}{\pi(R_a^4 - R_i^4)} r. \tag{12}$$

The elastic shear stresses reach the maximum at the outer radius $R_a = 4$ mm, with the inner radius $R_i = 2.4$ mm:

$$\tau_{max} = \tau(R_a) = \frac{2M_z R_a}{\pi(R_a^4 - R_i^4)} = \frac{M_z}{87.5 \text{ mm}^3} \tag{13}$$

with the equivalent von Mises stress $\sqrt{3}\tau_{max}$. In the FEM-based shakedown analysis the pipe is discretized with $n$ elements. The model uses 16 elements on the periphery, such that the yielding of the pipe starts for $\sigma_y = 485$ N/mm$^2$ at

$$M_z^e = 23.20 \text{ Nm}, \tag{14}$$

which is sufficiently close to the analytical value $M_z^e = 24.5$ Nm. In the case of an additional tension load the von Mises yield function $F$ has the following form:

$$F[\boldsymbol{\sigma}] = \sigma_r^2 + \sigma_\theta^2 + \sigma_z^2 - \sigma_r\sigma_\theta - \sigma_r\sigma_z - \sigma_\theta\sigma_z + 3\tau^2, \tag{15}$$

with the stresses $\boldsymbol{\sigma} = (\sigma_r, \sigma_\theta, \sigma_z, \tau)^T$. The overall constant elastic stresses $\boldsymbol{\sigma}_N$ are in equilibrium with the tension $N$,

$$\boldsymbol{\sigma}_N = (0, 0, \sigma_N, 0)^T \text{ and } \sigma_N = \frac{N}{\pi(R_a^2 - R_i^2)}. \tag{16}$$

For the stresses $\boldsymbol{\sigma}_N$ and $\boldsymbol{\sigma}_M$ equilibrating the tension $N_y = \alpha N$ and the constant moment $M_z$ it holds:

$$F[\alpha\boldsymbol{\sigma}_N + \boldsymbol{\sigma}_M] = (\alpha\sigma_N)^2 + 3\tau^2. \tag{17}$$

The maximal equivalent stress is obtained at the outer radius $R_a$, such that the yielding starts for the constant moment $M_z$ at the tension $N_y$ with:

$$N_y = \alpha_y N \text{ and } \alpha_y = \frac{\sqrt{\sigma_y^2 - 3\tau(R_a)^2}}{\sigma_N}. \tag{18}$$

The stress components of $\boldsymbol{\sigma}_N$ and $\boldsymbol{\sigma}_M$ are independent, such that the elastic domain is a 1/4 circle for a normalization by $M_z^e = 23.25$ Nm and $N^e = 15.60$ kN.

### 4.2. Limit analysis

The maximal allowable moment $M_{lim}$ and the maximal allowable tension $N_{lim}$ for perfectly plastic material with the yield stress $\sigma_y = 485$ N/mm$^2$ are given with the plastic limit factor $\eta_{pl}$ (Betten, 1985):

$$M_{lim}^{pp} = \eta_{pl} M_z^e = \frac{4}{3} \frac{1 - \left(\frac{R_i}{R_a}\right)^3}{1 - \left(\frac{R_i}{R_a}\right)^4} M_z^e = 1.20 M_z^e = 27.98 \text{ Nm}, \tag{19}$$

$$N_{lim}^{pp} = \pi(R_a^2 - R_i^2)\sigma_y = 15.62\text{kN}, \tag{20}$$

which fit exactly with the numerical values. For kinematic hardening material with the ultimate stress $\sigma_u = 631$ N/mm$^2$ with $\sigma_u/\sigma_y = 1.3$ it is

$$M_{lim}^{kin} = \sigma_u/\sigma_y M_{lim}^{pp} = 1.3 M_{lim}^{pp} = 36.37 \text{ Nm}, \tag{21}$$

$$N_{lim}^{kin} = \sigma_u/\sigma_y N_{lim}^{pp} = 1.3 N_{lim}^{pp} = 20.30 \text{ kN}. \tag{22}$$

The limit load domain for kinematic hardening material is a proportional enlargement of the perfectly plastic limit load domain by the factor $\sigma_u/\sigma_y = 1.3$.

### 4.3. Shakedown analysis for constant moment

The shakedown analysis for constant moment $M_z$ (dead load) and variable tension $N \in [0, N_{max}]$ with mean value $1/2N_{max}$ for unbounded kinematic hardening material with the free variables $\mathbf{y} = \boldsymbol{\rho} - \boldsymbol{\pi} = (\mathrm{y_r}, \mathrm{y}_\theta, \mathrm{y_z}, \mathrm{y_{rz}})^{\mathrm{T}}$ is given by

$$\begin{array}{ll} \max & \alpha \\ \text{s.t.} & F[\alpha\boldsymbol{\sigma}_N + \boldsymbol{\sigma}_M + \mathbf{y}] \le \sigma_y^2 \qquad \text{in all points} \\ & F[\boldsymbol{\sigma}_M + \mathbf{y}] \le \sigma_y^2 \qquad \text{in all points} \end{array} \tag{23}$$

$\boldsymbol{\sigma}_M$ and $\boldsymbol{\sigma}_N$ are with (12) and (16) in equilibrium with the loads $M_z$ and $N_y$, respectively. For every discretization with $n$ Gaussian points the stresses in the points $\boldsymbol{x}_j$ are given by:

$$\boldsymbol{\sigma}_M^j = (0, 0, 0, \tau^j)^T, \tag{24}$$

$$\boldsymbol{\sigma}_N^j = (0, 0, \sigma_N, 0)^T, \tag{25}$$

$$\mathbf{y}^j = (\mathrm{y_r^j}, \mathrm{y}_\theta^\mathrm{j}, \mathrm{y_z^j}, \mathrm{y_{rz}^j})^{\mathrm{T}}, \tag{26}$$

the Lagrangian of the optimization problem is given by (Fletcher, 1987):

$$L = -\alpha - \sum_{i=1}^{n} \lambda_{2i-1} \left\{ \sigma_y^2 - F[\alpha\boldsymbol{\sigma}_N^i + \boldsymbol{\sigma}_M^i + \mathbf{y}^i] \right\} - \sum_{i=1}^{n} \lambda_{2i} \left\{ \sigma_y^2 - F[\boldsymbol{\sigma}_M^i + \mathbf{y}^i] \right\} \tag{27}$$

with the Lagrange parameters $\lambda_l, l = 1, \ldots, 2n$. In the maximum the complementarity conditions hold for all $i = 1, \ldots, n$

$$0 = \lambda_{2i-1} \left\{ \sigma_y^2 - F[\alpha\boldsymbol{\sigma}_N^i + \boldsymbol{\sigma}_M^i + \mathbf{y}^i] \right\} \tag{28}$$

$$0 = \lambda_{2i} \left\{ \sigma_y^2 - F[\boldsymbol{\sigma}_M^i + \mathbf{y}^i] \right\}. \tag{29}$$

With $\nabla L(\alpha, \mathbf{y}^1, \ldots, \mathbf{y}^n) = \mathbf{0}$ it holds:

$$\frac{\partial L}{\partial \alpha} = 0 = -1 + \sum_{i=1}^{n} \lambda_{2i-1} \left\{ 2(\alpha\sigma_N^i + \mathrm{y_z^i})\sigma_\mathrm{N}^\mathrm{i} - \sigma_\mathrm{N}^\mathrm{i}\mathrm{y_r^i} - \sigma_\mathrm{N}^\mathrm{i}\mathrm{y}_\theta^\mathrm{i} \right\}. \tag{30}$$

and for all $i = 1, \ldots, n$:

$$
\begin{aligned}
0 &= [\lambda_{2i-1} + \lambda_{2i}] \left[2\mathrm{y}_{\mathrm{r}}^{\mathrm{i}} - \mathrm{y}_{\theta}^{\mathrm{i}} - \mathrm{y}_{\mathrm{z}}^{\mathrm{i}}\right] - \lambda_{2i-1}\alpha\sigma_N^i && (31)\\
0 &= [\lambda_{2i-1} + \lambda_{2i}] \left[2\mathrm{y}_{\theta}^{\mathrm{i}} - \mathrm{y}_{\mathrm{r}}^{\mathrm{i}} - \mathrm{y}_{\mathrm{z}}^{\mathrm{i}}\right] - \lambda_{2i-1}\alpha\sigma_N^i && (32)\\
0 &= [\lambda_{2i-1} + \lambda_{2i}] \left[2\mathrm{y}_{\mathrm{z}}^{\mathrm{i}} - \mathrm{y}_{\mathrm{r}}^{\mathrm{i}} - \mathrm{y}_{\theta}^{\mathrm{i}}\right] - 2\lambda_{2i-1}\alpha\sigma_N^i && (33)\\
0 &= (6\lambda_{2i-1} + 6\lambda_{2i})(\mathrm{y}_{\mathrm{rz}}^{\mathrm{i}} + \tau^{\mathrm{i}}) && (34)
\end{aligned}
$$

Without loss of generality we assume that in the maximum at least one Gaussian point $\boldsymbol{x}_j$ exists, such that either $\lambda_{2j-1} > 0$ or $\lambda_{2j} > 0$ holds (otherwise no point reaches the yield limit), such that from the conditions (31) and (32) follows $\mathrm{y}_{\mathrm{r}}^{\mathrm{j}} = \mathrm{y}_{\theta}^{\mathrm{j}}$. The following cases have to be considered:

i) $\underline{\lambda_{2j-1} = 0,\ \lambda_{2j} > 0}$:
With (31) and (33) follows $\mathrm{y}_{\mathrm{r}}^{\mathrm{j}} = \mathrm{y}_{\mathrm{z}}^{\mathrm{j}}$. With condition (34) it holds $\mathrm{y}_{\mathrm{rz}}^{\mathrm{j}} = -\tau^{\mathrm{j}}$ and conditions (29) gives a contradiction.

ii) $\underline{\lambda_{2j-1} > 0,\ \lambda_{2j} = 0}$:
With (33) follows $\alpha\sigma_N^j + \mathrm{y}_{\mathrm{z}}^{\mathrm{j}} = \mathrm{y}_{\mathrm{r}}^{\mathrm{j}}$. With condition (34) it holds $\mathrm{y}_{\mathrm{rz}}^{\mathrm{j}} = -\tau^{\mathrm{j}}$ and conditions (28) gives a contradiction.

iii) $\underline{\lambda_{2j-1} > 0,\ \lambda_{2j} > 0}$:

With (34) follows $\mathrm{y}_{\mathrm{rz}}^{\mathrm{j}} = -\tau^{\mathrm{j}}$. The complementarity conditions (28), (29) and $\alpha, \sigma_N^j > 0$ give

$$\alpha = \frac{\mathrm{y}_{\mathrm{r}}^{\mathrm{j}} + \mathrm{y}_{\theta}^{\mathrm{j}} - 2\mathrm{y}_{\mathrm{z}}^{\mathrm{j}}}{\sigma_N^j}. \tag{35}$$

Inserting this in condition (33) it yields $[\lambda_{2j-1} - \lambda_{2j}][\mathrm{y}_{\mathrm{z}}^{\mathrm{i}} - \mathrm{y}_{\mathrm{r}}^{\mathrm{i}}] = 0$ and $\lambda_{2j-1} = \lambda_{2j}$ (otherwise a contradiction is obtained from $\mathrm{y}_{\mathrm{z}}^{\mathrm{i}} - \mathrm{y}_{\mathrm{r}}^{\mathrm{i}} = 0$ and the condition (31). From the condition (31) follows $2(\mathrm{y}_{\mathrm{r}}^{\mathrm{j}} - \mathrm{y}_{\mathrm{z}}^{\mathrm{j}}) = \alpha\sigma_{\mathrm{N}}^{\mathrm{j}}$. Inserting this in condition (29) the shakedown factor $\alpha$ is obtained by:

$$\alpha = 2\frac{\sigma_y}{\sigma_N^j}. \tag{36}$$

For constant moment and cyclic tension the radius of the shakedown domain for unbounded kinematic hardening material is 2 times the radius of the elastic domain. This domain is larger than the limit load which is obtained in numerical shakedown analysis with FEM discretization using a bounded kinematic hardening model.

### 4.4. Shakedown analysis for constant tension

On the other hand the shakedown analysis for variable moment $M_z \in [0, M_{max}]$ with mean torque $1/2M_{max}$ and constant tension $N$ (dead load) for unbounded kinematic hardening material with the free variables $\mathbf{y} = \boldsymbol{\rho} - \boldsymbol{\pi} = (\mathrm{y_r}, \mathrm{y}_\theta, \mathrm{y_z}, \mathrm{y_{rz}})^{\mathrm{T}}$ is given by

$$
\begin{aligned}
\max \quad & \alpha \\
\text{s.t.} \quad & F[\alpha\boldsymbol{\sigma}_M + \boldsymbol{\sigma}_N + \mathbf{y}] \le \sigma_y^2 \qquad \text{in all points} \\
& F[\boldsymbol{\sigma}_N + \mathbf{y}] \le \sigma_y^2 \qquad \text{in all points}
\end{aligned} \tag{37}
$$

with the same stresses $\boldsymbol{\sigma}_M$ and $\boldsymbol{\sigma}_N$. For this load domain the following equation holds with (15):

$$
\begin{aligned}
F[\alpha\boldsymbol{\sigma}_M + \boldsymbol{\sigma}_N + \mathbf{y}] &= \mathrm{y}_r^2 + \mathrm{y}_\theta^2 + (\sigma_N + \mathrm{y}_z)^2 - \mathrm{y}_r\mathrm{y}_\theta - (\mathrm{y}_r + \mathrm{y}_\theta)(\sigma_N + \mathrm{y}_z) \\
&+ 3(\alpha\tau + \mathrm{y}_{rz})^2 \\
&= F[\boldsymbol{\sigma}_N + \mathbf{y}] + 3\alpha\tau(2\mathrm{y}_{rz} + \alpha\tau)
\end{aligned} \tag{38}
$$

The Lagrangian of the optimization problem is given by (Fletcher, 1987):

$$L = -\alpha - \sum_{i=1}^{n} \lambda_{2i-1} \left\{ \sigma_y^2 - F[\alpha \boldsymbol{\sigma}_M^i + \boldsymbol{\sigma}_N^i + \mathbf{y}^i] \right\} - \sum_{i=1}^{n} \lambda_{2i} \left\{ \sigma_y^2 - F[\boldsymbol{\sigma}_N^i + \mathbf{y}^i] \right\} \quad (39)$$

$$= -\alpha - \sum_{i=1}^{n} (\lambda_{2i-1} + \lambda_{2i}) \left\{ \sigma_y^2 - F[\boldsymbol{\sigma}_N^i + \mathbf{y}^i] \right\} + \sum_{i=1}^{n} \lambda_{2i-1} 3\alpha\tau^j (2\mathrm{y}_{\mathrm{rz}}^{\mathrm{j}} + \alpha\tau^{\mathrm{j}}) \quad (40)$$

with the Lagrange parameters $\lambda_l, l = 1, \ldots, 2n$. With $\nabla L(\alpha, \mathbf{y}^1, \ldots, \mathbf{y}^n) = \mathbf{0}$ it holds:

$$\frac{\partial L}{\partial \alpha} = 0 = -1 + \sum_{i=1}^{n} 6\lambda_{2i-1} (\alpha\tau^j + \mathrm{y}_{rz}^j)\tau^j \quad (41)$$

and for all $i = 1, \ldots, n$:

$$0 = [\lambda_{2i-1} + \lambda_{2i}] \left[ 2\mathrm{y}_{\mathrm{r}}^{\mathrm{i}} - \mathrm{y}_{\theta}^{\mathrm{i}} - (\sigma_{\mathrm{N}} + \mathrm{y}_{\mathrm{z}}^{\mathrm{i}}) \right] \quad (42)$$

$$0 = [\lambda_{2i-1} + \lambda_{2i}] \left[ 2\mathrm{y}_{\theta}^{\mathrm{i}} - \mathrm{y}_{\mathrm{r}}^{\mathrm{i}} - (\sigma_{\mathrm{N}} + \mathrm{y}_{\mathrm{z}}^{\mathrm{i}}) \right] \quad (43)$$

$$0 = [\lambda_{2i-1} + \lambda_{2i}] \left[ 2(\sigma_N + \mathrm{y}_{\mathrm{z}}^{\mathrm{i}}) - \mathrm{y}_{\mathrm{r}}^{\mathrm{i}} - \mathrm{y}_{\theta}^{\mathrm{i}} \right] \quad (44)$$

$$0 = 6\lambda_{2i-1} (\alpha\tau^j + \mathrm{y}_{rz}^j) + \lambda_{2i} 6\mathrm{y}_{rz}^j \quad (45)$$

Without loss of generality we assume that in the maximum at least one Gaussian points $\boldsymbol{x}_j$ exists, such that either $\lambda_{2j-1} > 0$ or $\lambda_{2j} > 0$ holds (otherwise no point reaches the yield limit), such that from the conditions (42) and (43) follows $\mathrm{y}_{\mathrm{r}}^{\mathrm{j}} = \mathrm{y}_{\theta}^{\mathrm{j}}$ and from (44) follows $\mathrm{y}_{\mathrm{r}}^{\mathrm{j}} = \sigma_{\mathrm{N}} + \mathrm{y}_{\mathrm{z}}^{\mathrm{j}}$. The complementarity conditions in the maximum are thus given by:

$$0 = \lambda_{2j-1} \left\{ \sigma_y^2 - 3(\alpha\tau^j + \mathrm{y}_{rz}^j)^2 \right\} \quad (46)$$

$$0 = \lambda_{2i} \left\{ \sigma_y^2 - 3(\mathrm{y}_{rz}^j)^2 \right\}. \quad (47)$$

The following cases have to be considered:

i) $\underline{\lambda_{2j-1} = 0, \lambda_{2j} > 0}$:
With (45) follows $\mathrm{y}_{\mathrm{rz}}^{\mathrm{j}} = 0$ and (47) gives a contradiction.

ii) $\underline{\lambda_{2j-1} > 0, \lambda_{2j} = 0}$:
With (45) follows $\alpha\tau^j + \mathrm{y}_{\mathrm{rz}}^{\mathrm{j}} = 0$ and (46) gives a contradiction.

iii) $\underline{\lambda_{2j-1} > 0, \lambda_{2j} > 0}$:
From condition (46) and (47) follows $\alpha = 0$ in contradiction to the assumptions.

For constant tension and cyclic moment with nonzero mean torque no elastic shakedown boundary can be defined for unbounded kinematic hardening. This situation can be resolved by introducing a bounding surface in the material model.

### 4.5. Shakedown interaction diagram

The shakedown domain for the FEM-model (Fig. 7) was computed by the basis-reduction method for the experimental conditions of constant torque and cyclic tension with nonzero mean stress. The interaction diagram (Fig. 8) is normalized by the pure shakedown tension $N_{z_0} = 15.62$ kN and by the pure shakedown moment $M_{z_0} = 27.98$ Nm for perfectly plastic material with $\sigma_y = 485$ N/mm$^2$. In the geometrically linear FEM shakedown analysis with the two-surface model of bounded linear kinematic hardening the shakedown domain and the limit load domain are the same. As a consequence no clear distinction between incremental and instantaneous collapse may be observed.

The interaction diagram shows a significant safety benefit for the kinematic hardening law in comparison to the perfectly plastic shakedown domain. Other examples for this effect (including thermally loaded structures) are given in (Heitzer et al., 2000).

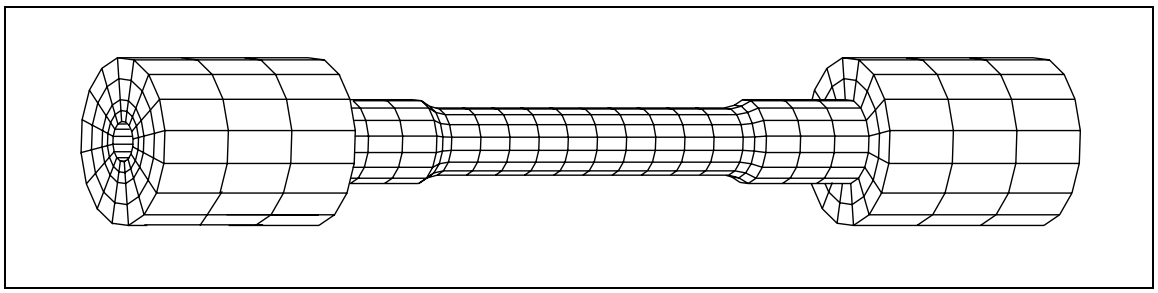

**Figure 7:** Finite element model

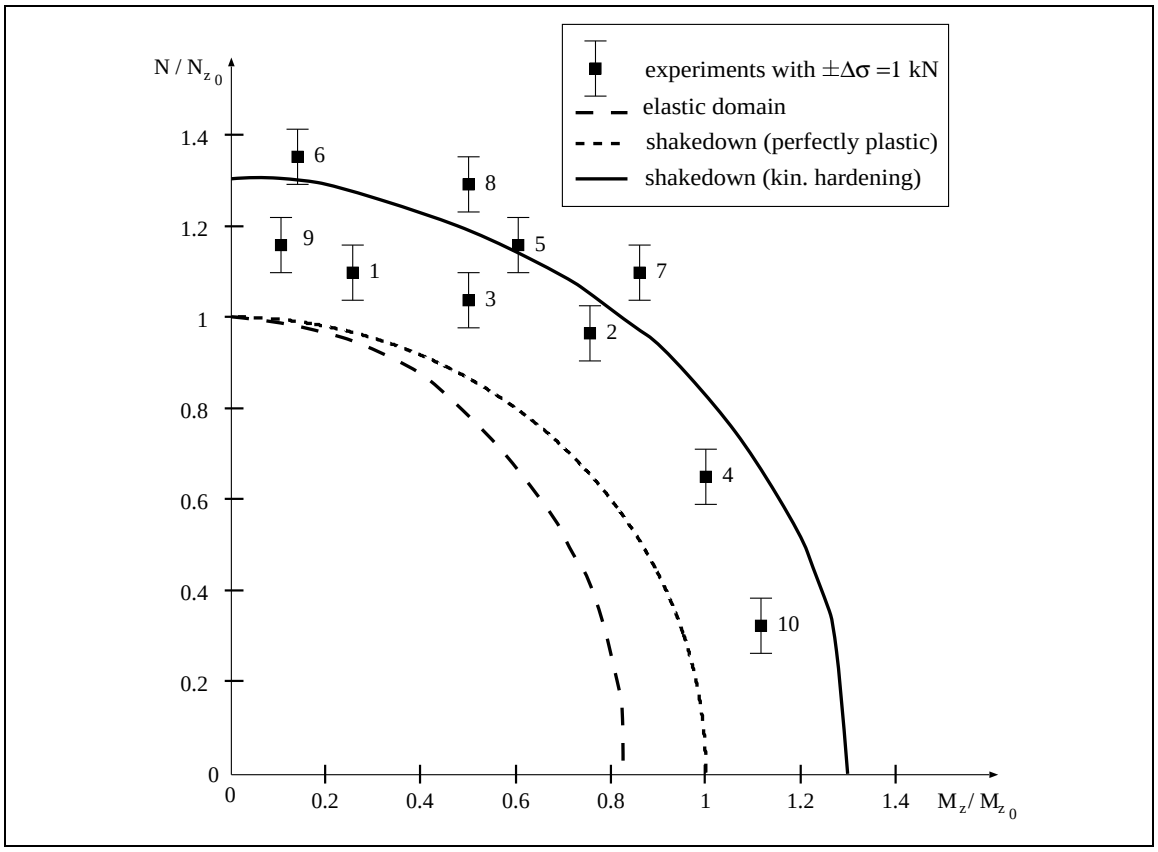


**Figure 8:** Shakedown interaction diagram and experimental data, normalized by the shakedown tension $N_{z_0}$ and shakedown moment $M_{z_0}$ for perfectly plastic material

### 4.6. Evaluation of the experiments

In the case of LCF and ratchetting the plastic strain increments do not vanish during the load history. This means that for elastic shakedown the plastic strains $\boldsymbol{\varepsilon}^p$ become stationary for the given load history, i.e. for $t \to \infty$ it holds

$$\lim_{t\to\infty} \dot{\boldsymbol{\varepsilon}}^p(x,t) = \mathbf{0} \;\text{ for all } x \in V. \tag{48}$$

To avoid the possibility of plastic failure the maximum possible plastic energy dissipation must be bounded above for all points of the structure. With an incremental computation it needs a lot of cycles to decide whether shakedown occurs or not. Therefore, a simple shakedown criterion (Wolters et al., 1996) can be derived, which can be used for the evaluation of the experiments. Let $n$ be the number of the loading cycles and $\dot{\boldsymbol{\varepsilon}}^p(n)$ the plastic strain increment at the end of the loading cycle $n$ in the weakest point of the structure. If the structure shakes down elastically the accumulation of all plastic strain increments must be bounded in this point,

$$\sum_{n=1}^{\infty} |\dot{\boldsymbol{\varepsilon}}^p(n)| < c. \tag{49}$$

With the axial strain $\varepsilon^p$ and the shear angle $\gamma^p = 2\varepsilon^p_{\theta z}$ the effective plastic strain increments are

$$|\dot{\boldsymbol{\varepsilon}}^p| := \sqrt{\frac{2}{3}\dot{\boldsymbol{\varepsilon}}^p : \dot{\boldsymbol{\varepsilon}}^p} = \sqrt{(\dot{\varepsilon}^p)^2 + \frac{4}{3}(\dot{\gamma}^p)^2}. \tag{50}$$

The shear angle $\gamma$ is calculated from the torsion angle $\vartheta$ on the length $L$ by

$$\gamma(r) = r\frac{\vartheta}{L}. \tag{51}$$

With a decomposition of the elastic and plastic strains (i.e. $\boldsymbol{\varepsilon} = \boldsymbol{\varepsilon}^e + \boldsymbol{\varepsilon}^p$), corresponding to the geometrical linear plasticity theory, the plastic strain increment $\dot{\gamma}^p$ are calculated by the differences at the same load. The simplest condition of the convergence of this sum as generalized harmonic series is the condition $|\dot{\boldsymbol{\varepsilon}}^p(n)| \le an^s$ with $s < -1$. This means in a double logarithmical diagram of the loading cycles and the plastic strain increments, that the slope must exceed $s = -1$ in the case of LCF or ratchetting. The results of the least square fit of the logarithmical data for the derived plastic strain increments of the measured data are shown in Tab. 4.

**Table 4:** Results of the simple extrapolation analysis

| Test No. | 1 | 2 | 3 | 4 | 5 | 6 | 7 | 8[2] | 9 | 10 |
|---|---|---|---|---|---|---|---|---|---|---|
| slope $s$ | -3.98 | -0.82 | -1.42 | -2.19 | -1.10 | -1.41 | -1.21 | -0.65 | -1.71 | -1.12 |

[2] Initial or intermediate overload, such that the strains for the interpolation have to be reduced.

From a first impression we expect from Fig. 4 ratchetting for experiment No. 2 and from Fig. 5 shakedown for experiment No. 4. From the values of $s$ the convergence of (49) can be deduced. the load levels 1,3,4,6,9 and with reservation 5 and 10 (probably an oversized torsion angle is obtained in the pre-test of experiment 10) are in the shakedown domain, because the plastic strains are bounded. For experiments No. 2 and 8 ratchetting has to be expected, because the plastic strains are unbounded. With respect to the experimental uncertainties this corresponds to the interaction diagram Fig. 8.

## 5. Material ratchetting

### 5.1. Linear and nonlinear kinematic hardening models

Structural shakedown analysis is designed to exclude structural ratchetting which is produced by inhomogeneous stress fields (Hübel, 1996). The tension torsion experiment is situated between

structural and material ratchetting, because the stress is the more homogeneous the thinner the tube wall is. Homogeneous fields are controlled by the behaviour of a representative material point. The analysis of uniaxial and biaxial stress cycles shows that the kinematic hardening is the primary reason for material ratchetting. Therefore, it is essential to develop and verify hardening rules which perform well under various cyclic loadings.

The Melan (1938) and Prager (1956) linear kinematic hardening law is known to be inadequate to simulate biaxial material ratchetting. The most well-known nonlinear kinematic hardening model has been proposed by Armstrong and Frederick (1966). Conceptually it is considered a leap in representing cyclic plasticity response of materials but not robust enough to predict the ratchetting response of materials (Bari, 2001). Later, cyclic plasticity models have been suggested, which needed uniaxial and multiaxial cyclic tests for material characterization. Then the best could predict the amount of ratchetting in experiments which are close to the tests used for parameter determination. But all known models fail on one or more material ratchetting experiments. The large class of so-called coupled models fail conceptually to represent biaxial ratchetting if the material parameters are matched to the uniaxial tests and vice versa, because the uniaxial hardening modulus cannot be chosen independently of the kinematic hardening (Bari, 2001). More flexibility is offered by the Dafalias and Popov (1975) two surface model. Common to all modern models is that they need many parameters, which have to be determined in several cyclic tests. Parameter determination is vague for some models. Other models need uniaxial or biaxial ratchetting tests or try to formulate the anisotropic deformation of the yield surface. Such effort is prohibitive for most industrial applications.

No comparative study of the multiaxial shakedown behaviour of different cyclic plasticity models is known. Shakedown analysis of cyclic structural plasticity needs only few characteristic material parameter and only the bounds of the load history. A similar benefit may be assumed for the analysis of cyclic material response. Below the two surface model for bounded kinematic hardening with a piecewise linear Melan and Prager law is compared with the nonlinear kinematic Armstrong and Frederick evanescence memory model which has been extended to multiple back stresses by Chaboche (Lemaître and Chaboche, 1990).

The original Melan and Prager model is characterized by unbounded linear kinematic hardening

$$F[\boldsymbol{\sigma} - \boldsymbol{\pi}] \leq \sigma_y^2, \tag{52}$$

$$\dot{\boldsymbol{\pi}} = \frac{2}{3} C \dot{\boldsymbol{\varepsilon}}^p = \frac{2}{3} \dot{\lambda} C \frac{\partial \sqrt{F}}{\partial \boldsymbol{\sigma}}, \tag{53}$$

with the associated plastic flow

$$\dot{\boldsymbol{\varepsilon}}^p = \dot{\lambda} \frac{\partial \sqrt{F}}{\partial \boldsymbol{\sigma}}. \tag{54}$$

The movement of the yield surface $F[\boldsymbol{\sigma}] \leq \sigma_y^2$ by the backstress evolution $\dot{\boldsymbol{\pi}}$ and the plastic flow $\dot{\boldsymbol{\varepsilon}}^p$ are both parallel and normal to the yield surface in this model. Backstress $\boldsymbol{\pi}$ and plastic strain $\boldsymbol{\varepsilon}^p$ are both deviators if $F$ is the von Mises function. The uniaxial hardening modulus is $H = C$. The linear kinematic hardening always stabilizes to shakedown of homogeneous stress fields after some initial overprediction of ratchetting (Bari, 2001). A more realistic model is obtained by restricting the movement of the yield surface such that it always stays inside a bounding surface which does not translate in stress space. This is achieved by the additional constraint

$$F[\boldsymbol{\sigma}] \leq \sigma_u^2, \tag{55}$$

which together with (52) implies

$$F[\boldsymbol{\pi}] \leq (\sigma_u - \sigma_y)^2. \tag{56}$$

From a monotonic tension test $\sigma_y$ and $\sigma_u$ may be identified by $R_{p0.2}$ and $R_m$, respectively. But for cyclic experiments material parameters from a stable hysteresis curve may be more appropriate if such data is available.

The Armstrong and Frederick model introduces a recall term $-\zeta\boldsymbol{\pi}|\dot{\boldsymbol{\varepsilon}}^p|$ for the fading memory

$$\dot{\boldsymbol{\pi}} = \frac{2}{3}C\dot{\boldsymbol{\varepsilon}}^p - \zeta\boldsymbol{\pi}|\dot{\boldsymbol{\varepsilon}}^p|, \tag{57}$$

with the non-associated plastic flow

$$\dot{\boldsymbol{\varepsilon}}^p = \dot{\lambda}\frac{\partial f}{\partial \boldsymbol{\sigma}}, \tag{58}$$

with

$$f = \sqrt{F[\boldsymbol{\sigma}-\boldsymbol{\pi}]} + \frac{3}{4}\frac{\boldsymbol{\pi}:\boldsymbol{\pi}}{\pi_u} \le \sigma_u. \tag{59}$$

The uniaxial hardening modulus is $H = C - \zeta\pi\text{sign}(\sigma-\pi)$. Then $\pi_u = C/\zeta$ denotes the ultimate shift of the center of the initial yield surface $F[\boldsymbol{\sigma}] = \sigma_y^2$ in a uniaxial tension test, such that $\sigma_u = \sigma_y + \pi_u$ and $F[\boldsymbol{\pi}] \le \pi_u^2$. This is again a two-surface model. The same bounding surface (55) is not postulated but it is assumed asymptotically by the kinematic evolution rule (57) with $\dot{\boldsymbol{\pi}}$ no more proportional to the plastic flow $\dot{\boldsymbol{\varepsilon}}^p$.

Let $\boldsymbol{n}$ be the outward normal to the yield surface at the current stress point $\boldsymbol{\sigma}$. Let $\boldsymbol{\sigma}_L$ be the stress state on the bounding surface with the same outward normal $\boldsymbol{n}$. Then it holds

$$\boldsymbol{n} = \frac{\boldsymbol{\sigma}_L^D}{\sigma_u} = \frac{\boldsymbol{\sigma}^D - \boldsymbol{\pi}}{\sigma_y}. \tag{60}$$

The model turns out to be a particular two-surface Mróz kinematic hardening model with a shift of the yield surface by

$$\dot{\boldsymbol{\pi}} = \zeta(\boldsymbol{\sigma}_L^D - \boldsymbol{\sigma}^D)|\dot{\boldsymbol{\varepsilon}}^p| \tag{61}$$

in deviatoric stress space.

### 5.2. Material shakedown analysis

In torsion experiments the stress is the more homogeneous the thinner the tube wall is. Any material point is representative for homogeneous stress fields. Therefore, ratchetting or shakedown are caused by the material behaviour due to the nonproportional loading and may be analyzed by consideration of the movement and deformation of the yield surface. Shakedown analysis is a simplified method which only considers the stabilized state and avoids the detailed analysis of the whole deformation process.

Consider a constant tension with $\sigma_N$ followed by a cyclic torsion with shear stress $\tau$. Plastic flow $\dot{\boldsymbol{\varepsilon}}^p = (\dot{\varepsilon}^p, \frac{1}{\sqrt{3}}\dot{\gamma}^p)$ starts if the stress point $\boldsymbol{\sigma} = (\sigma_N, \sqrt{3}\tau)$ lies on the yield surface. Cyclic 'creep' of the axial component $\dot{\varepsilon}^p$ stops if the yield surface touches the bounding surface in stress point $\sigma_L$. This elastic shakedown situation is constructed for the bounded Melan and Prager model and the Armstrong and Frederick model in Fig. 9 and Fig. 10. The stress points at shakedown are denoted $\sigma_{mp}$ and $\sigma_{af}$ for the Melan and Prager and the Armstrong and Frederick model, respectively. The figures also show the backstresses $\pi_{mp}$ and $\pi_{af}$ for both models at shakedown. For a constant torsion $\tau_N$ followed by a cyclic tension the same figures can be used to derive the material shakedown equations if the names of the axes are exchanged and the stress point $\boldsymbol{\sigma} = (\sigma, \sqrt{3}\tau_N)$ is considered.

This type of material ratchetting is covered by all kinematic hardening models (Hübel, 1996). But the originally unbounded Melan and Prager model ($\sigma_u \to \infty$) is quite unrealistic. For a cyclic loading with nonzero mean value no finite shakedown load and no finite limit load is found. In contrast to this, the material always shakes down for fully reversed cycles with a load amplitude at yield stress once the backstress has achieved the constant stress ($\sigma_N$ or $\tau_N$). For larger cycles damage is caused by LCF. Such strange behaviour has already been observed for structural shakedown in sections 4.2 and 4.3. Obviously the bounding surface $F[\boldsymbol{\sigma}] \le \sigma_u^2$ is the key to a realistic modeling of the shakedown behaviour.

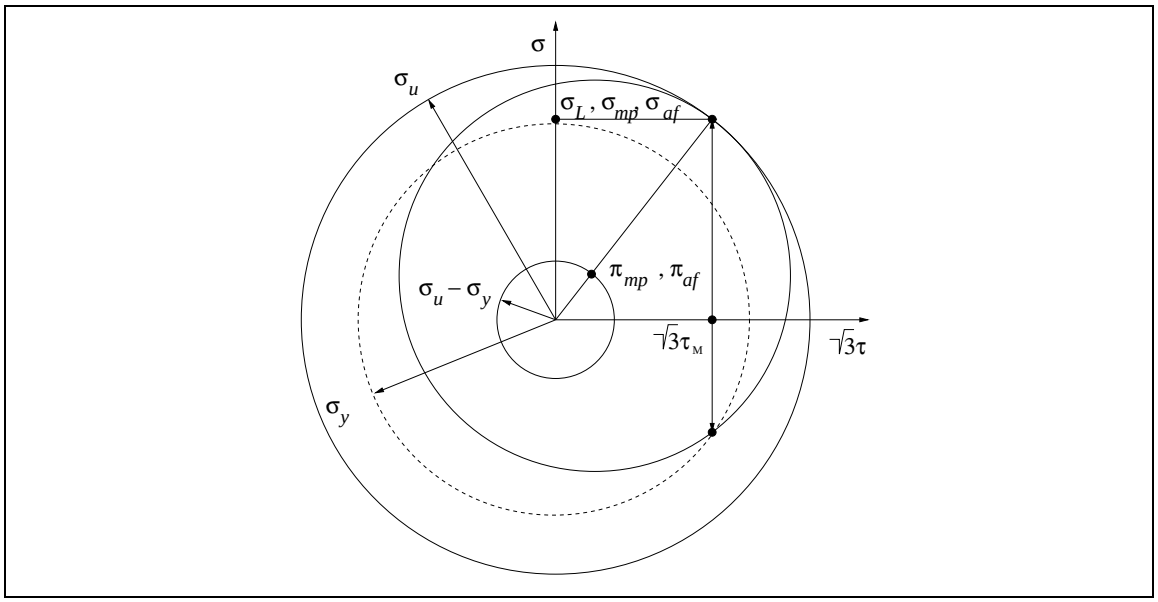


**Figure 9:** Constant tension and cyclic torsion with nonzero mean shear stress

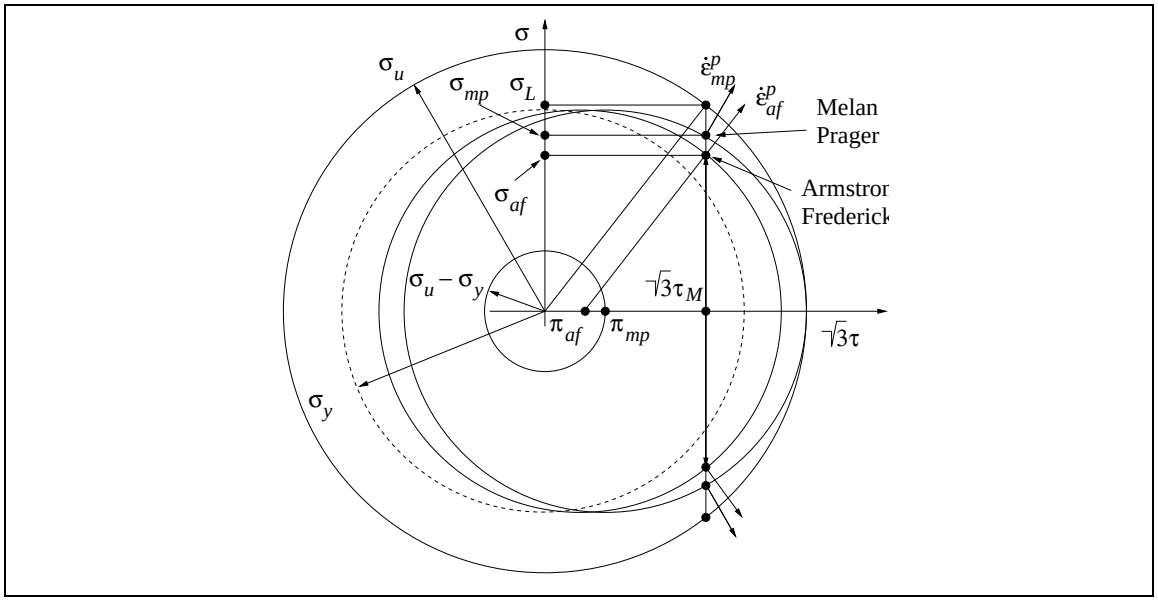


**Figure 10:** Constant tension and fully reversed torsion with zero mean shear stress

i) For the tension-torsion shakedown experiment with constant tension $\sigma_N$ and nonzero mean torsion Fig. 9 shows that both hardening models lead to the same material shakedown limit of the maximum shear stress $\tau_{max} < \tau_L$,

$$\tau_L = \frac{1}{\sqrt{3}}\sqrt{\sigma_u^2 - \sigma_N^2}. \tag{62}$$

The solution is valid for any cyclic torsion with a minimum shear stress $\tau_{min} > \tau_L(\sigma_u - 2\sigma_y)/\sigma_u$. For comparison with the structural shakedown this condition is depicted in the load space in the interaction diagram Fig. 8. The structural effect is most effective on the pure torsion axis. There is no difference between structural shakedown and material shakedown for the homogeneous stress state in pure tension. As observed for structural shakedown also the material shakedown stress coincides with the stress at instantaneous plastic collapse at limit load, because the points $\sigma_{mp}$ and $\sigma_{af}$ coincide with $\sigma_L$ on the bounding surface.

For an experiment with constant torsion $\tau_N$ and nonzero mean tension the shakedown limit of the maximum tension $\sigma_{max} < \sigma_L$ is

$$\sigma_L = \sqrt{\sigma_u^2 - 3\tau_N^2} \tag{63}$$

for both material models. The solution is valid for any cyclic tension with a minimum stress $\sigma_{min} > \sigma_L(\sigma_u - 2\sigma_y)/\sigma_u$ and it is identical to the limit load in the interaction diagram Fig. 11.

ii) A difference between the linear and the nonlinear kinematic hardening model may be observed in an experiment with fully reversed torsion cycles with zero mean shear stress ($\tau_{min} = -\tau_{max}$). For constant tension $\sigma_N$ the material shakedown condition for the bounded Melan and Prager model in Fig. 10 is

$$\tau_{mp} = \begin{cases} \frac{1}{\sqrt{3}}\sigma_y & \text{for} \quad 0 \le \sigma_N \le \sigma_u - \sigma_y, \\ \frac{1}{\sqrt{3}}\sqrt{\sigma_y^2 - (\sigma_N + \sigma_y - \sigma_u)^2} & \text{for} \quad \sigma_u - \sigma_y < \sigma_N \le \sigma_u. \end{cases} \tag{64}$$

For constant torsion $\tau_N$ and fully reversed tension with zero mean stress ($\sigma_{min} = -\sigma_{max}$) the material shakedown condition for the bounded Melan and Prager model is

$$\sigma_{mp} = \begin{cases} \sigma_y & \text{for} \quad 0 \le \sqrt{3}\tau_N \le \sigma_u - \sigma_y, \\ \sqrt{\sigma_y^2 - (\sqrt{3}\tau_N + \sigma_y - \sigma_u)^2} & \text{for} \quad \sigma_u - \sigma_y < \sqrt{3}\tau_N \le \sigma_u. \end{cases} \tag{65}$$

For the Armstrong and Frederick model a result of Lemaître and Chaboche (1990) is obtained for constant tension $\sigma_N$ and fully reversed torsion ($\tau_m = 0$) in Fig. 10

$$\tau_{af} = \frac{1}{\sqrt{3}}\frac{\sigma_y}{\sigma_u}\sqrt{\sigma_u^2 - \sigma_N^2} = \frac{\sigma_y}{\sigma_u}\tau_L. \tag{66}$$

It is derived from structural shakedown analysis in De Saxce et al. (2000). The material shakedown load is below limit load for both models except for pure tension. For pure shear no material shakedown may be achieved with amplitudes beyond $1/\sqrt{3}\sigma_y$ for both models.

For constant torsion $\tau_N$ and fully reversed tension ($\sigma_m = 0$) the result is

$$\sigma_{af} = \frac{\sigma_y}{\sigma_u}\sqrt{\sigma_u^2 - 3\tau_N^2} = \frac{\sigma_y}{\sigma_u}\sigma_L. \tag{67}$$

The material shakedown stress is below limit load for both models except for pure shear. For pure tension no material shakedown may be achieved with amplitudes beyond $\sigma_y$ for both models. This shakedown stress is presented in the interaction diagram Fig. 11.

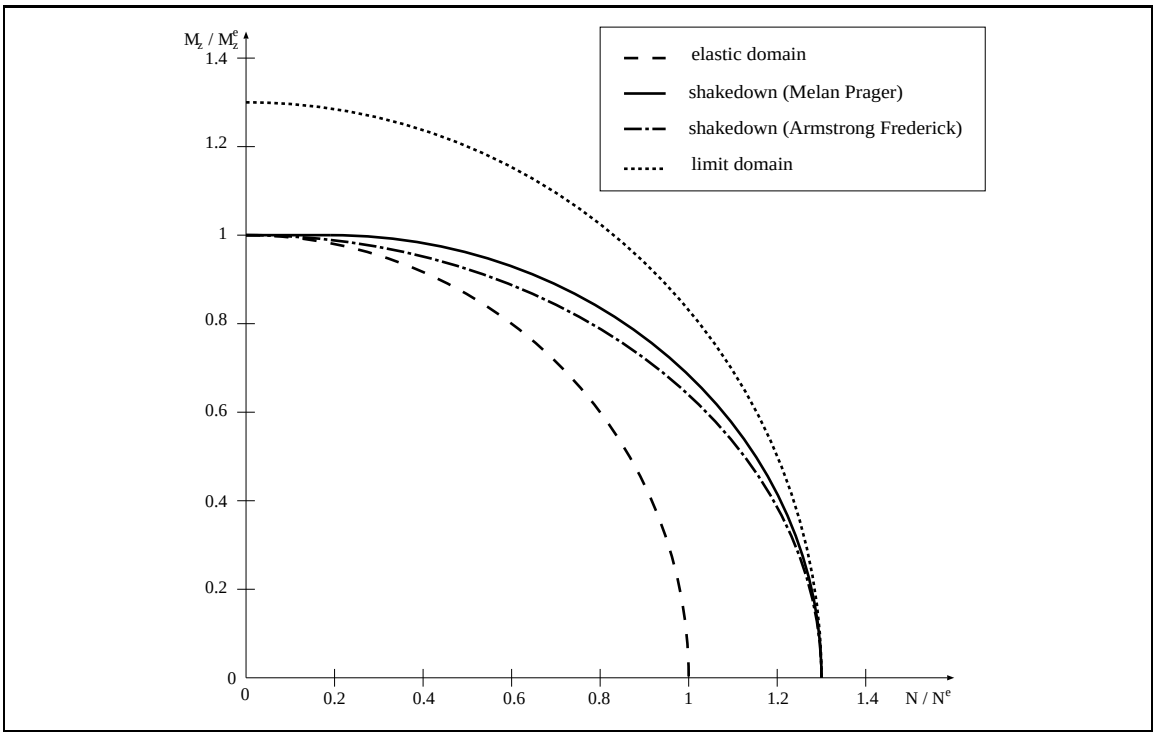


**Figure 11:** Material shakedown interaction diagram for fully reversed tension loading, normalized by the shakedown tension $N^e$ and shakedown moment $M_z^e$ for perfectly plastic material

On a material level elasticity is any history in the interior of the initial yield surface. The boundary of the purely elastic range $F[\boldsymbol{\sigma}] < \sigma_y^2$ can be read as the equation $\sqrt{3}\tau + \sigma = \sigma_y$ of the dotted circle in Fig. 9 and Fig. 10. The only difference between elasticity and elastic material shakedown is that the latter is any history in the interior of the shifted yield surface (loading surface). Therefore, a distinction can only be made if the nature of the surface is known. For this the backstress needs to be known with kinematic hardening models. But the backstress is not an observable quantity. Therefore, no difference between elastic shakedown and elasticity can be made in a continuum theory if the existence of a yield surface is accepted. On a continuum level the yield surface is most evident in metal plasticity in the discontinuous temperature evolution in a tension test (Gabryszewski and Sródka, 1986).

Material limit load is assumed if $F[\boldsymbol{\sigma}] = \sigma_u^2$. It is the solution of the equation $\sqrt{3}\tau + \sigma = \sigma_u$ of the outer circle in Fig. 9 and Fig. 10. Both hardening models predict material shakedown for cyclic stress with nonzero mean value up to material limit load. Both (62) and (63) make no distinction between unlimited ratchetting and plastic collapse for this biaxial loading. In contrast to it another behaviour shows up with fully reversed stress cycles. For both models separated stress regimes exist with distinct material behaviour: elastic, shakedown, ratchetting, and collapse. Similarly to structural shakedown analysis no details of the load history are needed and material characterization is simplified for the Armstrong and Frederick model. In tension torsion loading there is no or only little difference in the shakedown behaviour between a bounded linear and a nonlinear kinematic hardening material model. But the shakedown limits change noticeably with the load domains. This is also typically observed in structural shakedown analyses (see e.g. the interaction diagram of a pipe junction in Staat and Heitzer, 2001).

## 6. Summary

Limit and shakedown analyses are simplified but exact methods of plasticity, which do not contain any restrictive prerequisites apart from sufficient ductility. The simplifications concern the details

of material behaviour and of the load history. A simple tension-torsion experiment was performed comprising a hollow tension specimen which was subjected to alternating axial forces, superimposed with constant moments. The bounded linear kinematic hardening material model was applied to the shakedown analysis using the PERMAS program. It is shown that this shakedown analysis gives reasonable agreement between the experimental data, a simple estimation algorithm and the numerical results. With the kinematic hardening models a significant safety benefit is demonstrated in comparison to the perfectly plastic formulation. Further experimental validation with cyclic stabilized material data is needed before best use can be made of this safety potential. Additionally, the shakedown theory could be extended to more advanced hardening formulations. However, simple two-surface plasticity models produce realistic shakedown ranges. The linear and nonlinear kinematic hardening versions exhibit distinct ratchetting behaviour but they predict same or quite similar shakedown ranges. In contrast to this, the shakedown limits change noticeably with the load domains. Also the structural influence of a nonhomogeneous stress field may have a larger influence than the differences in the considered two-surface plasticity models.

*Acknowledgment:*
The research has been partly funded by the European Commission as part of the Brite–EuRam III project LISA: FEM–Based Limit and Shakedown Analysis for Design and Integrity Assessment in European Industry (Project N°: BE 97–4547, Contract N°: BRPR–CT97–0595).

## References:

Armstrong, P.J., Frederick, C.O., 1966. A Mathematical Representation of the Multiaxial Bauschinger Effect. Central Electricity Generating Board Report No. RD/BN/N 731.

Bari, S., 2001. Constitutive Modeling for Cyclic Plasticity and Ratcheting, Ph.D. Thesis, North Carolina State University, Raleigh.

Betten, J., 1985. Elastizitäts- und Plastizitätslehre, Vieweg, Braunschweig, Wiesbaden.

Dafalias, Y. F., Popov, E. P., 1975. A model of nonlinearly hardening materials for complex loading. Acta Mechanica 21, 173–192.

De Saxce, G., Tritsch, J.-B., Hjiaj, M., 2000. Shakedown of elastic-plastic structures with non-linear kinematical hardening by the bipotential approach. in Weichert, D., Maier, G. (Eds.): Inelastic Analysis of Structures under Variable Loads, Kluwer, Dordrecht, 167–182.

Fletcher, R., 1987. Practical Methods of Optimization, John Wiley & Sons, New York.

Gabryszewski, Z., Sródka, W., 1986. Thermal Effects during the Deformation of Gray, Cast Iron. International Journal of Solids and Structures 22,

Heitzer, M., 1999. Traglast- und Einspielanalyse zur Bewertung der Sicherheit passiver Komponenten, Berichte des Forschungszentrums Jülich, Jül–3704.

Heitzer, M., Pop, G., Staat, M., 2000. Basis reduction for the shakedown problem for bounded kinematic hardening material. Journal of Global Optimization 17, 185-200.

Heitzer, M., Staat, M., 1999. FEM–computation of load carrying capacity of highly loaded passive components by direct methods. Nuclear Engineering and Design 193, 349–358.

Hübel, H., 1996. Basic Conditions for Material and Structural Ratcheting. Nuclear Engineering and Design 162, 55-65.

Intes, 1988. PERMAS User's Reference Manuals, Stuttgart, Intes Publications No. 202, 207, 208, 302, UM 404, UM 405.

Lang, H., Wirtz, K., Heitzer, M., Staat, M., Oettel, R., 2001. Cyclic Plastic Deformation Tests to Verify FEM-Based Shakedown Analyses. Nuclear Engineering and Design 206, 227-239.

Lemaitre, J., Chaboche, J.–L., 1990. Mechanics of Solid Materials, University Press, Cambridge.

Melan, E., 1938. Zur Plastizität des räumlichen Kontinuums, Ingenieur–Archiv 8, 116–126.

Prager, W., 1956. A New Method of Analyzing Stresses and Strains in Work Hardening Plastic Solids. Journal of Applied Mechanics 23, 493–496.

Ponter, A.R.S., 1983. Shakedown and Ratchetting below the Creep Range, CEC Report EUR 8702 EN, Brussels.

Portier, L., Calloch, S., Marquis, D., Geyer, P., 2000. Ratchetting under tension-torsion loadings: experiments and modelling. International Journal of Plasticity 16, 303–335.

Pycko, S., Maier, G., 1995. Shakedown theorems for some classes of nonassociated hardening elastic-plastic material models. International Journal of Plasticity 11, 367–395.

Staat, M., Heitzer, M., 2001. LISA a European Project for FEM-based Limit and Shakedown Analysis. Nuclear Engineering and Design 206, 151–166.

Stein, E., Zhang, G., Mahnken, R., 1993. Shakedown analysis for perfectly plastic and kinematic hardening materials, in Stein, E. (ed.): Progress in computational analysis of inelastic structures, Springer, Wien, 175–244.

Taylor, N. et al., 1999. The Design-by-Analysis Manual, CEC Report EUR 19020 EN, DG-JRC/IAM, Petten.

Wolters, J., Breitbach, G., Rödig, M., 1996. Untersuchungen zum Ratchetting von Segmenten der Ersten Wand zukünftiger Fusionsreaktoren unter zyklischer thermischer und mechanischer Belastung, Berichte des Forschungszentrums Jülich, Jül–3250.